Steel and Composite Structures, *Vol. 36, No. 4* (*2020*) *447-462*
DOI: https://doi.org/10.12989/scs.2020.36.4.447

Influence of stiffeners on the performance of blind-bolt end-plate connections to CFST columns

Fa-xing Ding[1,2], Zhi-cheng Pan[1], Peng Liu*[1,2], Shi-jian Huang[1], Liang Luo[3] and Tao Zhang[4]

[1]*School of Civil Engineering, Central South University, Changsha, Hunan Province, 410075, PR China*
[2]*Engineering Technology Research Center for Prefabricated Construction Industrialization of Hunan Province, 410075, PR China*
[3]*School of Civil Engineering and Architecture, Nanchang Hangkong University, Nanchang, Jiangxi Province, 330036, PR China*
[4]*School of Civil Architecture, Zhengzhou University of Aeronautics, Zhengzhou, Henan Province, 450000, PR China*

(*Received May 16, 2019, Revised July 11, 2020, Accepted July 28, 2020*)

Abstract. The paper aims to investigate the mechanical mechanism and seismic effect of stiffeners in blind bolt endplate connection to CFST column. A precise 3D finite element model with considering the cyclic properties of concrete and steel materials was established, and the efficiency was validated through monotonic and cyclic test data. The deforming pattern and the seismic performance of the unstiffened and stiffened blind bolt endplate connections were investigated. Then a parametric analysis was conducted to analyze the contribution of stiffeners and the joint working behaviors with endplate under cyclic load. The joint stiffness classifications were compared and a supplement stiffness classification method was proposed, and the energy dissipation ability of different class connections were compared and discussed. Results indicated that the main deformation pattern of unstiffened blind bolt endplate connections was the local bending of end plate. The vertical stiffeners can effectively alleviate the local bending deformation of end plate. And influence of stiffeners in thin endplate and thick endplate was different. Based on the stiffness of external diaphragm welded connection, a more detailed rigidity classification was proposed which included the pin, semi-rigid, quasi-rigid and rigid connection. Beam was the main energy dissipation source for rigid connection. For the semi-rigid and quasi-rigid connection, the extended endplate, stiffeners and steel beam would all participate in the energy dissipation.

Keywords: concrete filled steel tube (CFST); endplate connections; high-strength blind bolts; finite element (FE) analysis; energy dissipation; rigidity classification

1. Introduction

The end-plate bolted connection involves shop-welding the beam end to steel plates which are then field-bolted to the connecting members, then the welding work can be limited and a good connecting quality can be guaranteed. Therefore, due to the advantages of simple construction and economy fabrication and erection, the end-plate bolted connections have been widely applied in the steel frame structures in Europe, the United States and many Asian countries (D'Aniello *et al*. 2017, Morrison *et al*. 2017, Wang *et al*. 2018, Ma *et al*. 2011). Researches on end-plate bolted connections in Europe and American countries started early and the analyses are mainly around connections to wide flange or H section columns. Da Silva (2004) described experimental and numerical results on flush end-plate beam-to-column joints to try to review the current 10% limitation imposed by Eurocode 3 for joints subject to axial forces. Current experimental tests of extended end-plate joints subjected to bending moment and axial force should provide additional clarification of these issues. Dessouki (2013) conducted a series of numerical simulations on extended end-plate connections, and found that the majority of these connections behaved as the semi-rigid connections and the moment bearing ability mainly depended on the thickness of the end plate and the diameter of bolts. Beena (2017) established finite element researches on bolted connections, and the results were compared with experimental results found that the proposed CFST beam-column connections perform in a semi-rigid and partial strength mode as per specification of EC3.

Since the endplate bolted connections generally display relative low stiffness and strengths, some stiffening measures are often adopted and the stiffened end-plate connections strengthened by rid plates on both tension and compression sides are commonly adopted for seismic applications. Several experimental and numerical researches have proved that the rid stiffener can effectively influence the stress and deformation pattern at the endplate connections. The bolt force distribution was more uniform and the end plate deformations as well as prying forces were reduced with the addition of the diagonal stiffeners (Tsai *et al*. 1990, Tartaglia *et al*. 2018). The stiffened endplate connections can be theoretically designed to be of either full or partial strength and full or semi-rigid depending on the details of rid stiffeners (Wang *et al*. 2018, Guo *et al*. 2006). The findings and results of related studies have provided useful guidance to the development and application of end-plate bolted connections (D'Aniello *et al*.

*Corresponding author, Ph.D.
E-mail: lop868@163.com

Copyright © 2020 Techno-Press, Ltd.

ISSN: 1229-9367 (Print), 1598-6233 (Online)

(a)Slip-Critical Blind Bolt proposed by Wang *et al* (2017).

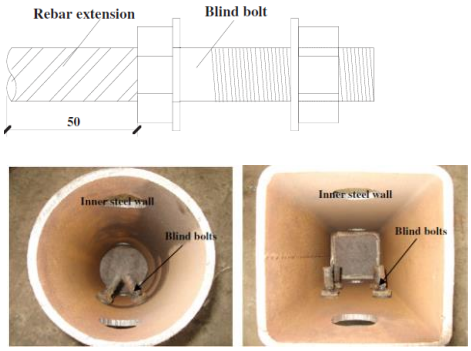

(b)Blind Bolts proposed by Wang *et al* (2013).

Fig. 1 Examples of blind bolts

2017, A. AISC 2010, Murray 2003, EC3 2005, Tartaglia *et al*. 2018).

Above mentioned studies and findings are all around end-plate bolted connections to wide flange or H shaped columns. While in many Asian countries or in certain steel buildings, the concrete filled steel tube (CFST) columns are generally adopted. The closed section and two side-webs construction in CFST columns will lead to different internal stress transmission patterns as compared to similar connections to H-shaped columns (Suita *et al.* 2000, Yu *et al.* 2015), then leading to different deformation patterns and yield line mechanism (Wang and Wang 2016). Moreover, the closed section construction of steel tube in CFST columns will bring difficulties on the bolt installation, due to the inaccessibility of the internal space of the tube. Then the long through bolts are often applied for the end-plated bolted connections to CFST columns (Tao *et al*. 2017). In recent years, another bolting system that developed to realize the end-plate connection to CFST columns is the blind bolt connections. These blind bolt fasteners can be accessed and installed from only one side of the plate (i.e. from the outside of column tube), thus providing a convenient connecting work onsite (Fig. 1), as in the case of connecting the end plate of a beam to a tube column.

Nowadays many kind of blind bolts have been proposed and studied like Ajax-Oneside bolt (Waqas *et al*. 2019), Flowdrill (Yao *et al*. 2008), Hollo-bolt (Wang *et al*. 2018) and Slip-Critical Blind Bolt (Wang *et al*. 2017). These blind bolts use different mechanisms to achieve the one-side installation, and therefore different connection performance are presented. Mourad et al. carried out monotonic tests (Korol *et al*. 1993) and cyclic tests (Mourad *et al*. 1995) on endplate connections with blind oversized mechanically locked (BOM) fasteners for the flexural behaviors. (Thai *et al*. 2017, Wang *et al*. 2018) performed a series of connection tests and frame tests on the performance of blind bolted endplate composite connections to CFST columns. The tested joints behaved in a semi-rigid manner but with satisfactory ductile behaviors. Wang *et al*. (2013) once carried out experimental studies on the mechanical behaviors of the flush or blind bolted endplate joints to square and circular CFST columns. The monotonic loading and hysteretic behaviors of blind-bolt end-plate bolted connection to normal CFST and thin wall plate CFST columns were all tested (Wang and Spencer 2013, Wang *et al*. 2012, 2013). Results indicated that the blind bolt endplate connection can be of partial strength or full strength depending on the connection details like thickness of end-plate, column type and bolt diameters *et al*. Later, further studies have been applied to the seismic performance of blind bolt assembly CFST frames, and the frame presented preferable hysteretic behavior, ductility and energy dissipation (Zhang *et al*. 2019). However, from the point of stiffness, the connections were classified as semi-rigid type, and can only be applied in low and middle rise buildings.

In general, researches on the blind-bolt end-plate connections to CFST columns still stay at primary stages when compared to similar connections to H-shaped columns. More in-depth investigations like effect of stiffeners, design classifications and application guidance are still limited. A precise numerical model has been developed and the efficiency has been validated through the detailed comparisons with experimental work by Wang *et al.* (2012, 2013), to carry out further parametric study beyond the range of test specimens. Therefore, this paper introduces the investigation of mechanical performance of stiffeners in blind bolt endplate connection to rectangular CFST columns through finite element approaches. The effect of end plate thickness and stiffener thickness, and their influencing pattern to connection performance have been investigated. The stiffness and seismic performance have been evaluated based on a traditional external diaphragm joint, and a new suggestion on connection rigidity classification method is proposed.

2. Finite element model and analysis

2.1 Test description

In this paper, the FE models of the blind bolt endplate connection to CFST column were verified against the experimental results reported by Wang *et al*. (2012, 2013). A total of two monotonic tests (MES1 and MES2) and two quasi-static cyclic tests (DES1 and DES2) have been

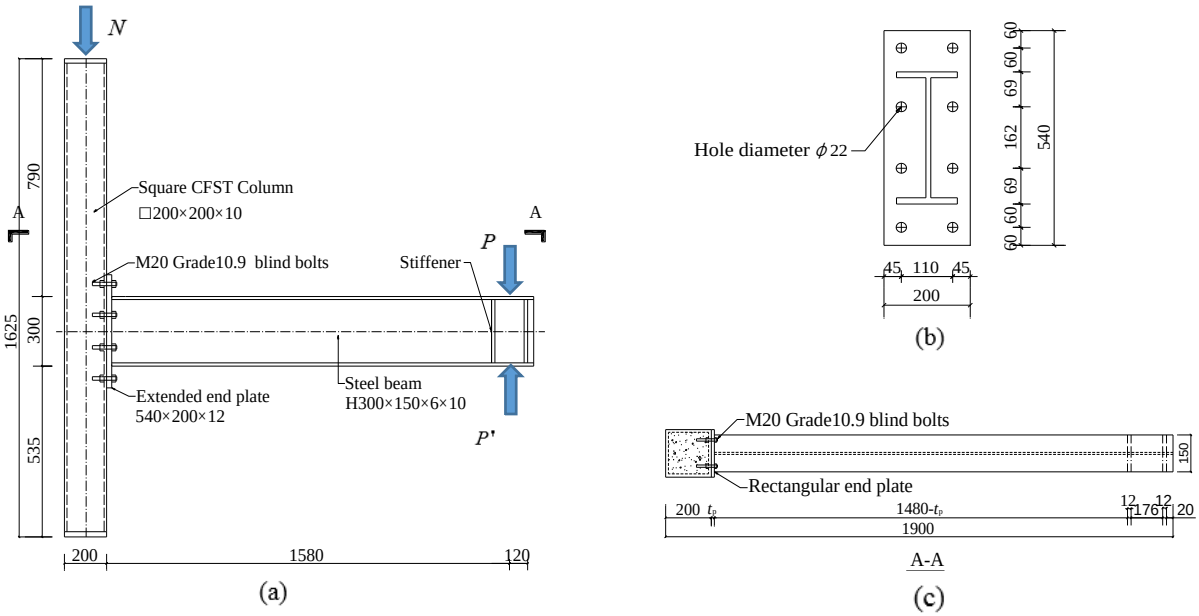

Fig. 2 Details of square CFST connection specimens

Table 1 Measure information of specimens

Specimens label	MES1/DES1	MES2/DES2
$D\times t$ (mm)	□200×10	□200×10
$h_b\times t_w\times t_f\times b_f$ (mm)	300×150×6×10	300×150×6×10
H (mm)	1625	1625
L (mm)	1700	1700
t_p (mm)	12	18

Table 2 Material properties

Specimens number	Thickness (mm)	f_y (N/mm^2)	f_u (N/mm^2)	E_s (N/mm^2)	δ (%)
Square steel tube	10	349.3	492	1.87×10^5	16.5
Beam flange	10	349.3	492	1.87×10^5	16.5
Beam web	6	312.5	508.3	2.16×10^5	17.4
Endplate-1	12	323.3	436.7	1.98×10^5	31.0
Endplate-2	18	274.4	414.4	1.93×10^5	24.8

performed on blind bolt connections, and the detailed dimension of the specimens and set-up can be found in Fig. 2. The difference between the two specimens under the same loading protocol (Wang *et al*. 2012, 2013) was the thickness of end plate (t_p =12 mm or 18 mm). The specimens were representative of exterior beam-to-column joints thus only one I-beam ($h_b\times t_w\times t_f\times b_f$) was blind bolted to the CFST column, and vertical displacement load was applied through the actuator installed at beam end. Table 1 summarize the dimension details of tested specimens, where D is the outer edge length of the cross-section of column; t is the wall thickness of steel tube; H is the height of column; L is the length of beam.

The extended end-plate was fastened to the rectangular CFST column with 8 high-strength blind bolts of Grade 10.9 M20 (Fig. 2(b)), with the yield strength and the ultimate strength as 940 N/mm^2 and 1040 N/mm^2, respectively. The modulus of elasticity was 2.05×10^5 N/mm^2 and the Poisson's ratio was 0.3. Material properties of steel components were measured through tension tests and are given in Table 2, where f_y and f_u are respectively the yield and ultimate stress of steel. δ is the elongation of steel; E_s is the elastic modulus of steel. The concrete strength was obtained through the 150 mm wide cube test and the average measured cube compressive strength (f_{cu}) and elastic modulus (E_c) of concrete were 44.34 N/mm^2 and 3.35×10^4N/mm^2, respectively.

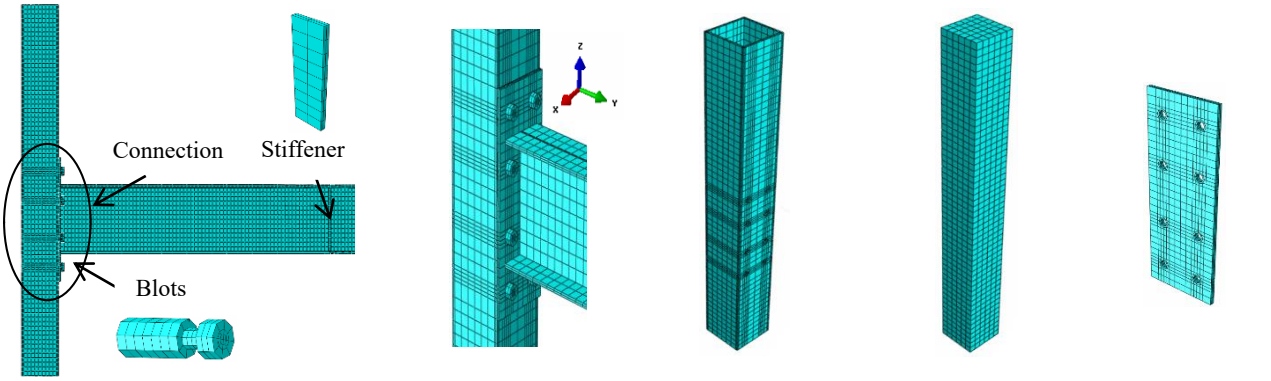

(a) Finite element model (b)Connection (c)Steel tube (d)Concrete core (e) End plate

Fig. 3 Finite element model of the studied connection

2.2 Finite element modeling

2.2.1 Material models

In this analysis, the damage plasticity model was employed to describe the constitutive behaviour of the infill concrete in CFST column. The unified constitutive model proposed by Ding *et al*. (2011a) was used, which can describe the concrete strength development under both tension and compression state with a unified calculation formula (Eq. (1)).

$$y=\begin{cases}\dfrac{A_n x+(B_n-1)x^2}{1+(A_n-2)x+B_n x^2} & (x\le 1)\\ \dfrac{x}{\alpha_n(x-1)^2+x} & (x>1)\end{cases} \tag{1}$$

where A_n is the ratio of the initial tangent modulus to the secant modulus of concrete material skeleton curve at peak stress; B_n controls the decrease of elastic modulus along the ascending portion of the axial stress-strain relationship; the parameter α_n controls descent phase of skeleton curves. For the uniaxial compressive case, n=1, $y=\sigma/f_c$ and $f_c=0.4f_{cu}^{7/6}$. Here σ is the real-time stress, f_c is the peak compression stress and f_{cu} is the axial compressive strength. Moreover, $x=\varepsilon/\varepsilon_c$, here ε is the real-time strain, ε_c is the peak compression strain and $\varepsilon_c=383f_{cu}^{7/18}\times10^{-6}$. Under this uniaxial compressive case, other parameter can be calculated as $A_1=9.1f_{cu}^{-4/9}$, $B_1=1.6(A_1-1)^2$, and $\alpha_1=0.15$ for concrete core in the column. For the uniaxial tensile case, n=2, then $y=\sigma/f_t$, here the f_t is the axial tension strength, and can be calculated as $f_t=0.24f_{cu}^{2/3}$. In this case, $x=\varepsilon/\varepsilon_t$. Here ε_t is the peak tensile strain and can be calculated as $\varepsilon_t=33f_{cu}^{1/3}\times10^6$. In this tension case, A_2=1.306, $B_2=5(A_2-1)^2/3$ = 0.15; and α_2=0.8.

Some other parameters for the plastic-damage constitutive model were defined by Ding *et al*. (2011a), as follows: the ratio of the second stress invariants on the tensile and compressive meridian was 2/3; the dilation angle was 40 degrees; the eccentricity ratio was 0.1. When the concrete was biaxially isostatic, the ratio of initial equibiaxial compressive strength to initial uniaxial compressive strength was 1.225; the viscosity coefficient was 0.005; the Poisson's ratio of concrete was set to 0.2; and the damage factor of concrete modulus was calculated with referencing of the concrete damage theory proposed by Ding *et al*. (2011a).

For the steel material, two different sets of constitutive models were adopted. In the numerical simulation of monotonic loading tests, the bilinear ideal elastoplastic model was applied for steel plate components like the steel tube, steel beams, end plates and stiffeners. The high strength bolts adopted a trilinear elastoplastic model with the strength growth changed at yield strain ε_y of 0.456% and at the ultimate strain ε_u of 10%. Since the steel materials will behave differently between monotonic loading and cyclic loading due to the cyclic hardening and Bauschinger effect (Yu *et al*. 2017), a different set of constitutive models, namely combined hardening model based on Chaboche theory, was adopted for the cyclic loading test simulations (Ding *et al*. 2017, 2017, 2018). The yield stress at zero plastic strain and the equivalent stress parameter were determined by the measured yield strength in Table 2, and other parameters for the cyclic hardening model was set referring to Ding *et al*. (2017, 2018). The kinematic hardening parameter Gamma and C1 was settled as 50 and 7500 respectively. The Q-infinite was settled as half of the yield strength and the isotropic hardening parameter b was 0.1.

2.2.2 Finite element model establishment

The eight-node 3D solid element C3D8R with reduced integral format were used to model the concrete and the steel parts like square steel tube, steel beam and high strength blind bolts. The element uses the reduced integration mode and the hourglass control to avoid the spurious solutions that resulted from shear locking and hourglass. Mesh convergence studies were also conducted to obtain a reasonable mesh which provided reliable results with less computational time, and then the final adopted finite element mesh for different part of studied connections are given in Fig. 3. The contact interaction between different components is simulated with surface-to-surface contact in ABAQUS. Then the bonding, frictional sliding and separation behaviors can all be modelled. The normal pressure relation was ensured through hard contact pressure

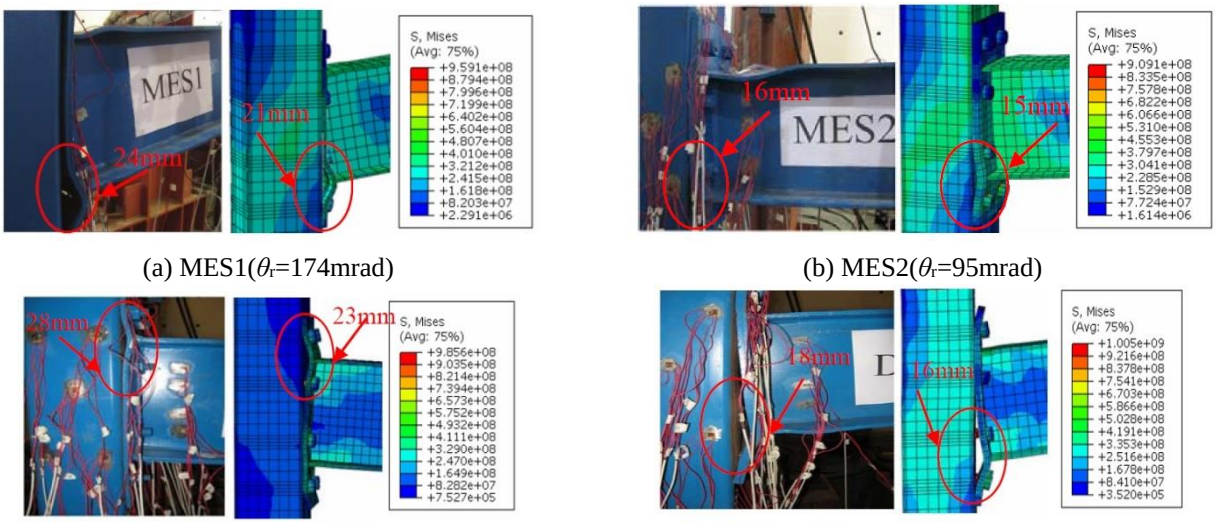

(a) MES1(θ_r=174mrad) (b) MES2(θ_r=95mrad)

(c) DES1(θ_r=101mrad) (d) DES2(θ_r=103mrad)

Fig. 4 Comparison of test and FEA failure modes of two connection specimens

model, and the Coulomb friction in the tangential direction was simulated with the PENALTY tangential function in the surface contact. The friction coefficient of 0.5 has been successfully used to simulate CFST columns (Ding *et al* 2017, 2018). Therefore, the friction coefficient of 0.5 for contact between steel tube and the core concrete, and was 0.45 for contact between steel parts. Both material and geometric nonlinearities are considered in the analyses and the Newton-Raphson incremental interaction method is used in the solution.

2.2.3 Boundary condition and loading mode

In the test, the column was constrained at the top and bottom end with hinge joint to simulated the inflection point location of the upper story column and bottom story column. Then in the finite element model, a consistent boundary setting was applied. The nodes at each column end were coupled to a central point. Then the displacement freedoms along X, Y, and Z direction of the bottom point were all constrained, and the X and Y direction displacements and rotational freedom around Z axis were constrained for the central point of the top section. A pretension force of 155 kN was applied to the shank section of high strength blind bolts through BOLT LOAD option available in ABAQUS, and the extension at bolt shank was fixed during the following loading steps. Then the constant axial load (with an axial compression ratio of 0.6) was exerted on the top of the CFST column, followed with the monotonic or cyclic displacement load applied to nodes at beam end section. The displacement loading process was consistent with the test.

2.3 Experiment validation

2.3.1 Failure mode

The precision of the FE models was validated through the comparison to experimental results. Fig. 4 gives the failure mode of the four joints from both experimental tests and numerical simulations (θ_r, is the change in angle between the centre lines of the beam and the column). The deformation pattern and failure modes of blind bolt endplate connection from the numerical simulations were consistent with the test results, for both monotonic loading and cyclic loading cases. All four connections behaved with similar failure mode, which included local buckling at extended end-plate, local buckling at beam flange, and yielding or fracture failure of tensile bolts. The rectangular CFST columns displayed outward deformation at the tension region of the side-plate. Connections with thinner end-plate tended to produce larger local bending deformation at the junction region with tensioned flange. The thicker endplate cases tend to have higher level of local buckling extent at beam flanges.

2.3.2 Comparison of moment-rotation relations

Fig. 5 gives the comparison of moment-rotation curves (M-θ_r) of tested connections between numerical simulations and test data. Results indicated that the finite element models can well predict the stiffness and strength development of blind bolt endplate connections, for both monotonic loading cases and cyclic loading cases. The finite element models displayed slightly higher strength during the yielding state of connection in monotonic loading cases. For cyclic loading conditions, the numerical model also present faster strength development and a bit higher strength growth during the transition period from elastic to plastic state. The finite element models can well predict the plasticity development and strength degradation during large displacement loading steps. Connection MES2 showed higher moment strength but earlier failure than that of MES1. Furthermore, Specimen DES2 displayed pinching behaviours during latter degradation stages when compared to Specimen DES1, which reflect the bolt slippage and the end plate deformation. The reasons for this difference mainly came from both a loss of bolt pretension force with

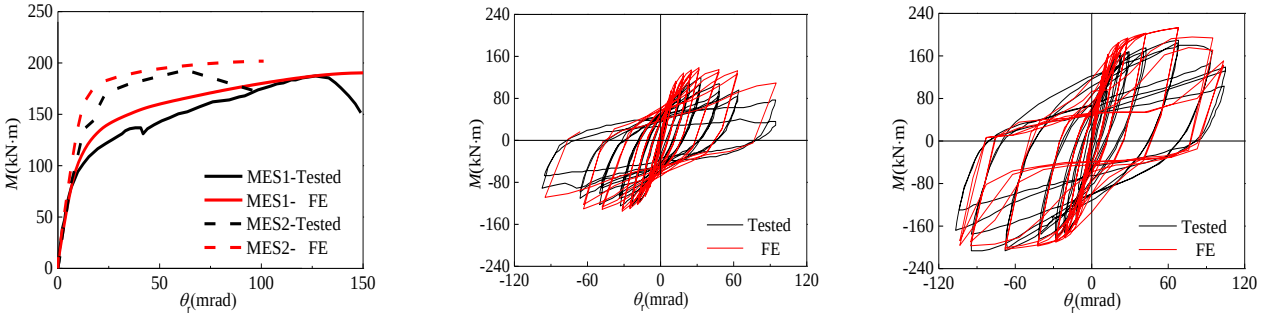

(a) Specimen MES1 and MES2 (b) Specimen DES1 (c) Specimen DES2

Fig. 5 Comparison of moment(M) versus rotation(θ_r) hysteretic curves

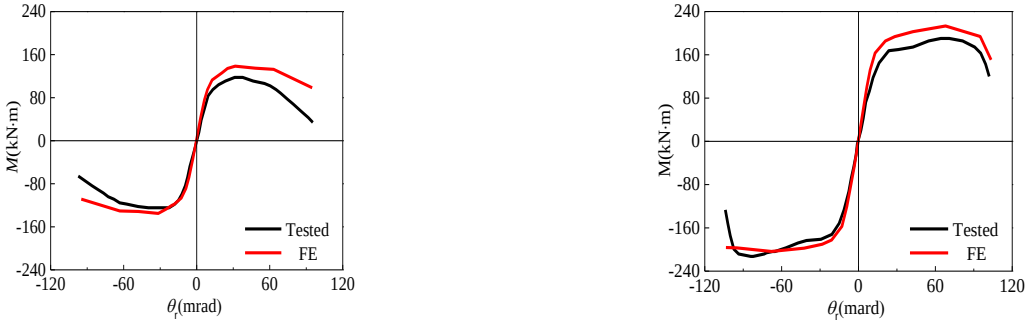

(a) Specimen DES1 (b) Specimen DES2

Fig. 6 Comparison of moment (M) versus rotation (θ_r) hysteretic curves

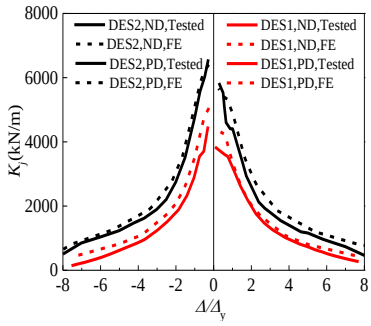

Fig. 7 Comparison with rigidity degradation curves

the loading cycles and the permanent deformation of the column wall or the end plate.

2.3.3 Comparison of envelope curve and rigidity degradation

Figs. 6 and 7 shows the moment-rotation (M-θ_r) skeleton curves and the stiffness degradation of the test data and FE simulations. The finite element model can basically predict the strength development along positive and negative direction, and shows that the stiffness homogeneous decreased with the increasing displacement. The FEM represents the ideal conditions without considering the initial defects in connection components and the set up. Therefore, the initial rotational stiffness and the ultimate moment capacity from numerical simulations are are slightly larger than the experimental test.

2.3.4 Comparison of moment-strain curves

During the test, strain gauges were mounted at different steel components to capture the strain development and internal stress state in the connections. Then these strain data were used to validate the internal stress distribution predicted from finite element models. Fig. 8 illustrates the comparison of strain development conditions versus the connection moment at the junction section. The specific location of each gauging point can be found in reference (Wang and Spencer 2013, Wang *et al*. 2013). It can be found that the established finite element model can also capture the strain development in the connection.

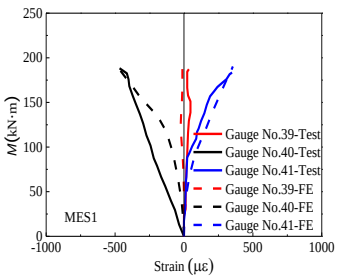

(a) Steel tube wall strain (MES1)

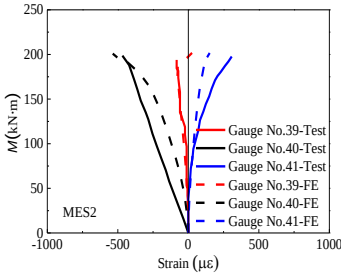

(b) Steel tube wall strain (MES2)

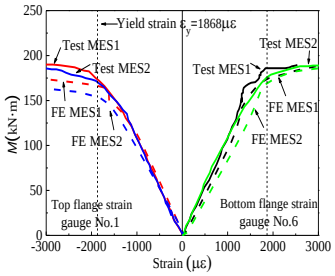

(c) Steel tube wall strain (MES1 and MES2)

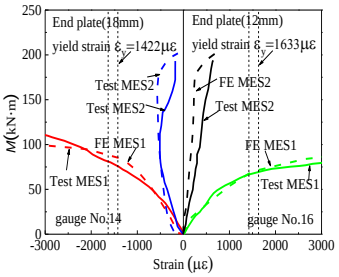

(d) End plate strain (MES1 and MES2)

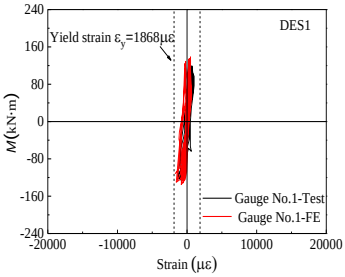

(e) Beam top flange strain (DES1)

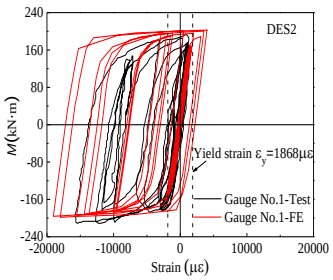

(f) Beam top flange strain (DES2)

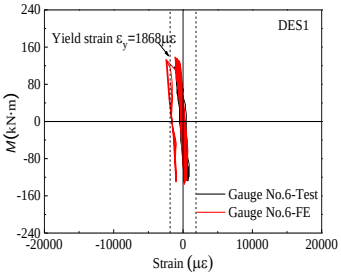

(g) Beam bottom flange strain (DES1)

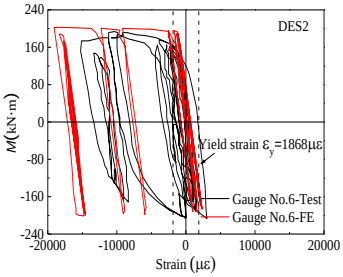

(h) Beam bottom flange strain (DES2)

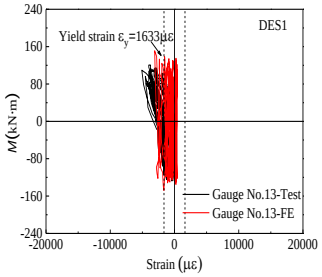

(i) End plate strain (DES1)

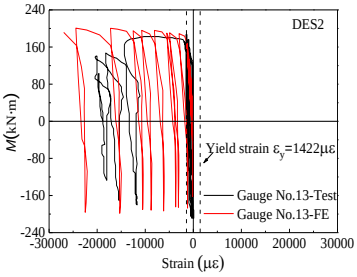

(j) End plate strain (DES2)

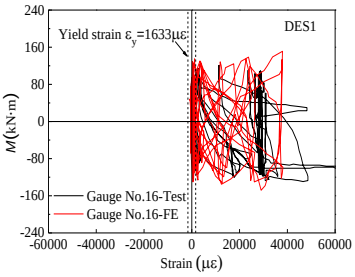

(k) End plate strain (DES1)

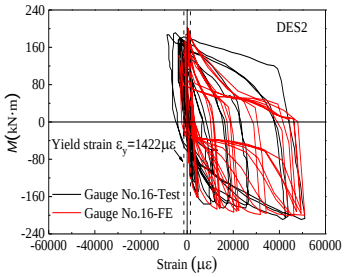

(l) End plate strain (DES2)

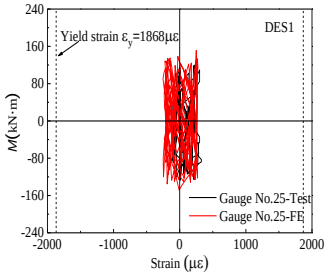

(m) Steel tube strain (DES1)

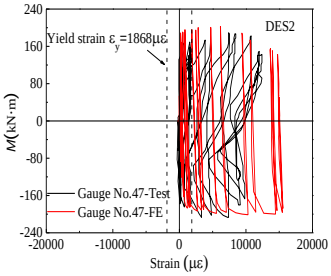

(n) Steel tube strain (DES2)

Fig. 8 Comparison of strain at different steel components

Table 3 Connection information of various models

Model number	Beam-column connection form	t_p (mm)	t_s (mm)	H (mm)	L (mm)	Connection perspective	Connection perspective
DES3		12	8				
DES4	End plate with stiffener	12	10			Fig.9(b)	Fig.9(a)、10(b)
DES5		12	12				
DES6	Unstiffened	14	0			Fig.2(c)	Fig.2(a)、10(a)
DES7		14	6				
DES8	End plate with stiffener	14	8			Fig.9(b)	Fig.9(a)、10(b)
DES9		14	10	1625	1700		
DES10	Unstiffened	16	0			Fig.2(c)	Fig.2(a)、10(a)
DES11	End plate with stiffener	16	6			Fig.9(b)	Fig.9(a)、10(b)
DES12		16	8				
DES13	End plate with stiffener	18	6			Fig.9(b)	Fig.9(a)、10(b)
DES14		18	8				
DES15	External diaphragm	/	/			Fig.9(d)	Fig.9(c)、10(c)

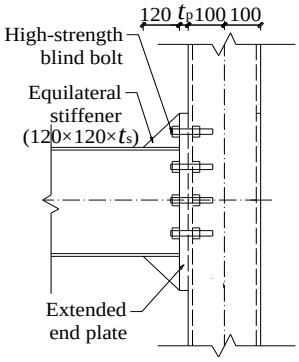

(a) End plate stiffener connection

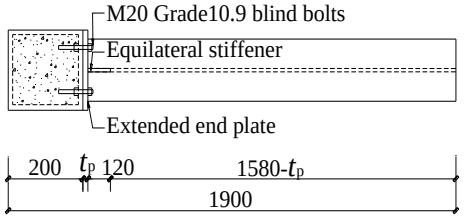

(b) End plate stiffener connection

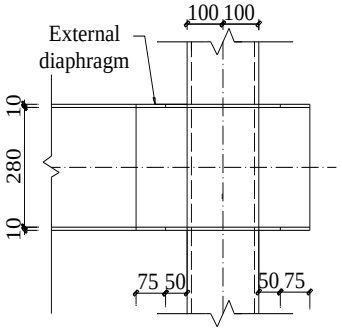

(c) External diaphragm

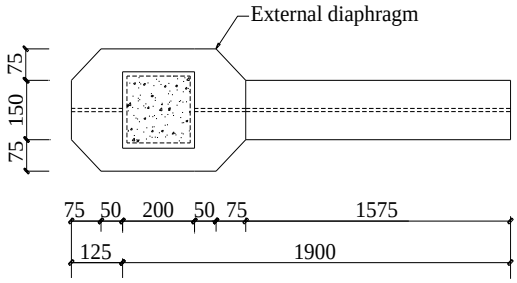

(d) External diaphragm

Fig. 9 Dimension and detail of model examples DES3~DES15

Furthermore, the plastic strains in the tested connection mainly happened at beam flanges and endplates, which were consistent with the failure modes and stress distributions in Fig. 4. Therefore, above comparisons proved the effectiveness of the finite element models in predicting the mechanical properties of blind bolt extended end-plate connections.

3. Analysis and evaluation of stiffened end-plate joint

3.1 Design of stiffened end-plate joint

The deformation pattern and failure modes of the blind-bolt end-plate connection displayed dramatic local bending and buckling at the endplate. Previous researches on extended endplate connections to H columns proved that an

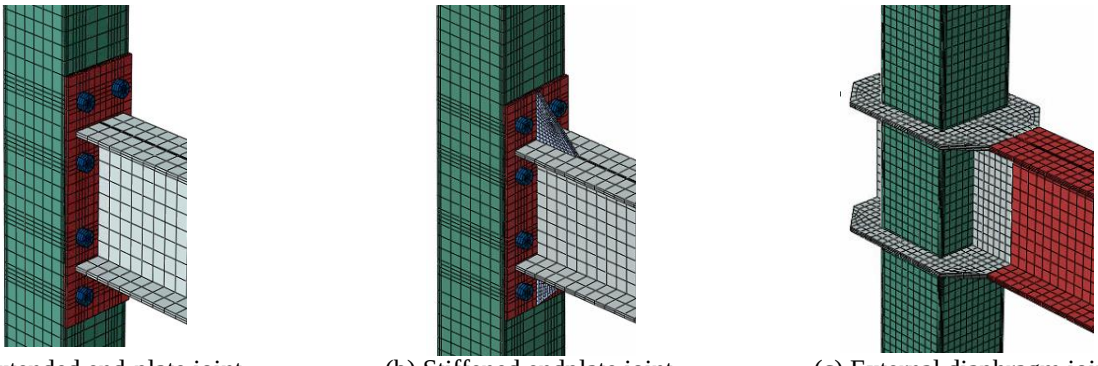

(a) Extended end-plate joint (b) Stiffened endplate joint (c) External diaphragm joint

Fig. 10 Finite element model of typical example joints

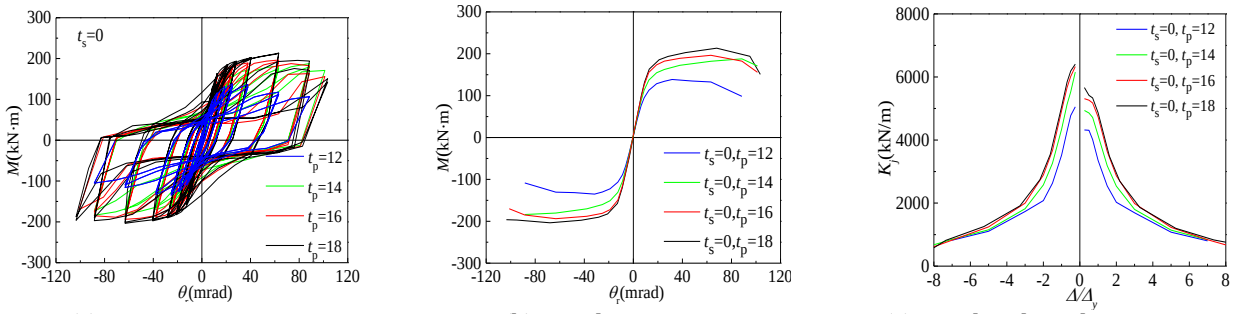

(a) Hysteretic curves (b) Envelope curves (c) Rigidity degradation curves

Fig. 11 The influence of thickness of unstiffened end plate

effective measure to reduce the endplate bending and to improve the connection behaviours was adding diagonal stiffeners at extended sides. Then in this analysis, the blind-bolt end-plate stiffeners connections were designed and studied based on the validated finite element modelling method. Figs. 9(a) and 9(b) and Fig. 10(b) present the construction of stiffened connection, in which triangular rid plates were welded to the center of the upper and bottom extended regions. To investigate the effect and influencing pattern of stiffeners, external diaphragm and endplates with different thicknesses were considered and the overall performance were compared to get a comprehensive evaluation of the blind-bolt end-plate connection. Then ten additional finite element endplate connection models were established. Moreover, to better compare the performance of stiffened connection, an external diaphragm connection was also established as the reference joint (Figs. 9(c) and 9(d) and Fig. 10(c)), which was often sorted as rigid joint in structural design. A total of 15 connection models were established with the detail construction parameters given in Table 3, where t_p is the end plate thickness, t_s is the stiffener thickness, H is the column height, L is the beam length. Then the cyclic loading analyses were performed to get the seismic behaviours. The section of CFST column was 200×200×8 mm, and the steel beam was H300×150×6×10 mm for all the studied connections.

3.2 Parametric studies

3.2.1 Effect of end plate thickness for unstiffened blind-bolt connections

The effect of end-plate thickness on the overall performance of unstiffened blind-bolt connections was studied at first. Here the thickness of end-plate varied from 12 mm to 18mm with the other constructional dimensions kept the same. The hysteretic behavior, skeleton curve and connection stiffness degradation were obtained and compared, as given in Fig. 11 and Table 6. It can be seen that: (1) For the unstiffened blind-bolt connections, the moment-rotation (M-θ_r) hysteresis loops displayed certain pinching behaviors, especially at larger loading cycles. (2) Fig. 12 gives the deformation conditions of unstiffened connection with different thickness endplate. The deformation at the connection region mainly presented the local bending and warping at endplate. Therefore, the moment bearing ability was increased with the increase of endplate thickness. But as the thickness got larger than 14 mm, the improving extent of the moment bearing ability was less prominent. (3) The endplate thickness would also influence the initial bending stiffness of the connection. The thicker the plate thickness, the greater the initial rotational stiffness of the joint. For example, compared to the joint DES1 (t_s=0, t_p=12), the positive and negative initial rotational stiffnesses of joint DES2 (t_s=0, t_p=18) were increased by 25.9% and 24.6%, respectively. (4) The

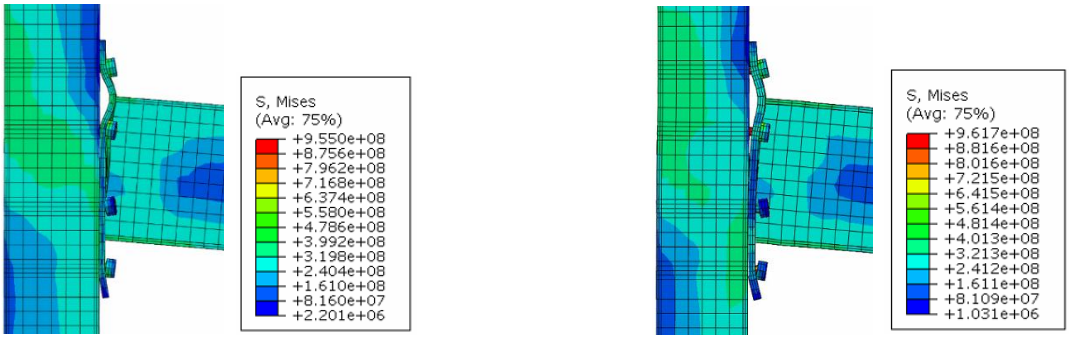

(a) (t_s=0, t_p=12) (b) (t_s=0, t_p=16)

Fig. 12 The influence of thickness of unstiffened end plate

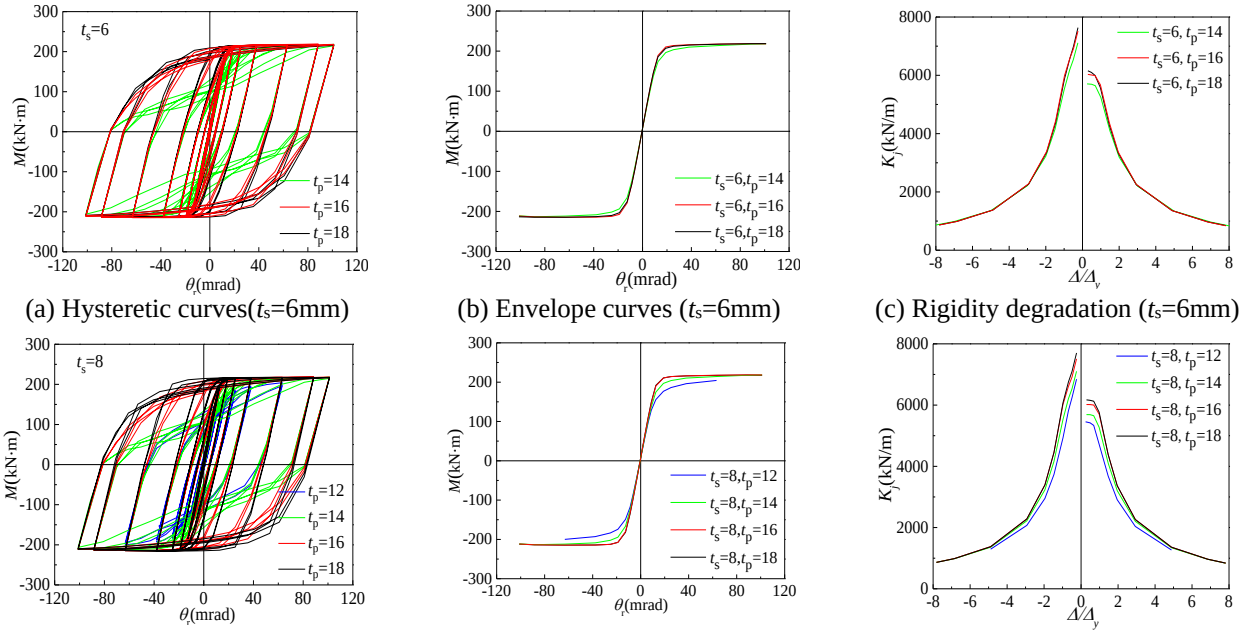

(a) Hysteretic curves(t_s=6mm) (b) Envelope curves (t_s=6mm) (c) Rigidity degradation (t_s=6mm)

(d) Hysteretic curves(t_s=8mm) (e) Envelope curves (t_s=8mm) (f) Rigidity degradation (t_s=8mm)

Fig. 13 The influence of thickness of stiffened end plate

endplate thickness mainly influenced the early stiffness degradation stage of the connection, while the residual connection stiffness tended to be the same in larger loading cycles.

3.2.2 Effect of endplate thickness for stiffened blind-bolt connections

In this part, the triangular stiffeners were added to the endplate, and totally two thicknesses were considered, which was 6 mm and 8 mm. Fig. 13 gives the comparison of hysteretic curves, skeleton curve and the stiffness degradation conditions. With the strengthening effect of vertical stiffeners, the moment-rotation hysteretic curves got more pump, and in thick endplate cases (t_p=16 and t_p=18) the connection displayed nearly full hysteretic loops. For connections with 6mm stiffeners, the skeleton curves and stiffness degradation of connections with different endplate were nearly the same. For thicker stiffener cases (t_s=8), slight differences were presented between connections with thinner (t_p≤14) and thicker endplate (t_p>14). The different moment bearing performance can be illustrated from the deformation pattern and failure mode given in Fig. 14. The presence of stiffener could effectively alleviate the internal stress distribution and local bending deformation at endplate. In large loading cycles, the stiffeners participated the energy dissipation though plasticity development, thus producing the relative pump hysteretic loops. In 14 mm endplate condition, there still had local bending deformation happened at the endplate, thus there still had slight pinching behaviors. For thicker endplate connections, the presence of stiffeners can well avoid the warping deformation at the endplate, resulting the pump moment-rotation hysteretic loops.

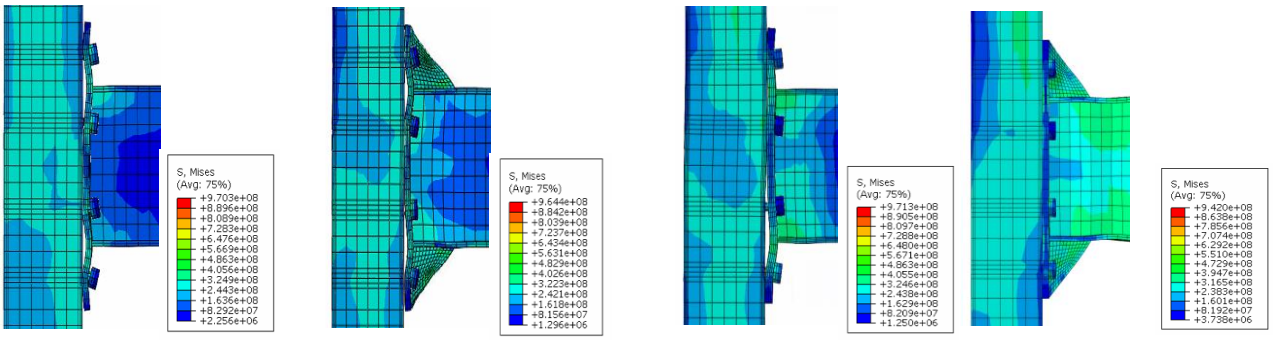

(a) (t_s=0, t_p=14) (b) (t_s=6, t_p=14) (c) (t_s=0, t_p=18) (d) (t_s=6, t_p=18)

Fig. 14 The influence of thickness of stiffened end plate

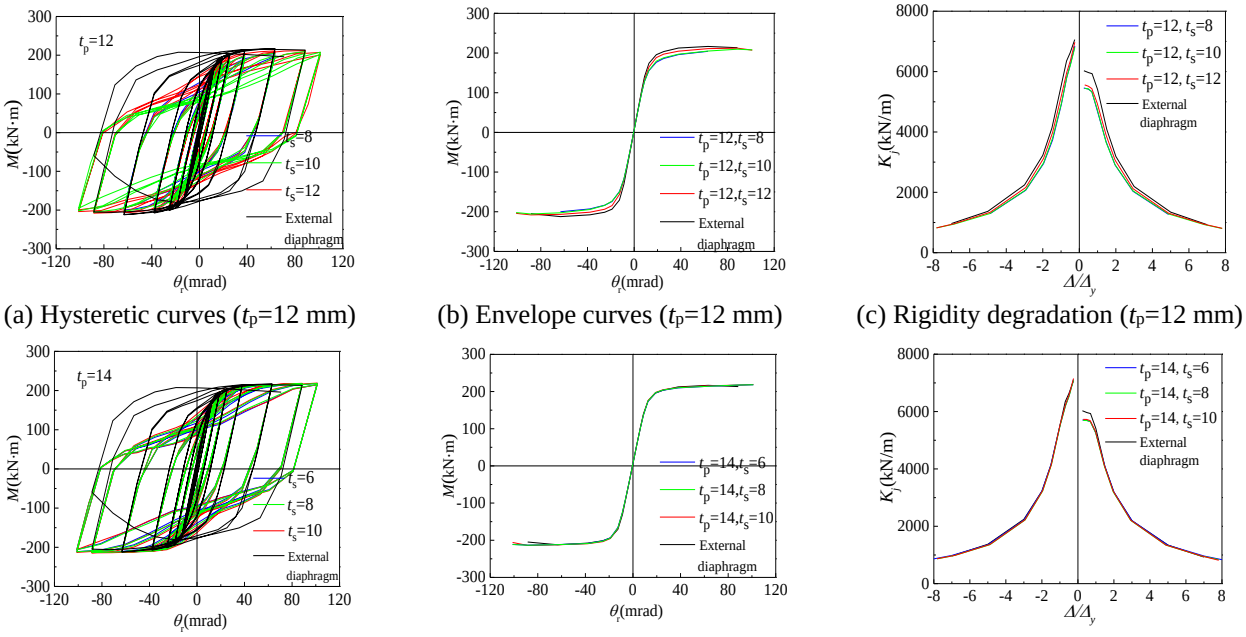

(a) Hysteretic curves (t_p=12 mm) (b) Envelope curves (t_p=12 mm) (c) Rigidity degradation (t_p=12 mm)

(d) Hysteretic curves (t_p =14 mm) (e) Envelope curves (t_p =14 mm) (f) Rigidity degradation (t_p =14 mm)

Fig. 15 The influence of stiffener thickness for thin end plate

3.2.3 Effect of stiffener thickness for thin end plate blind-bolt connections

In previous discussion it can be indicated that the performance of stiffened blind bolt connections was closely related to the combined effect of stiffeners and the endplate. Furthermore, the deformation pattern and failure modes were also different between thinner endplate connections and the thicker endplate connections. Therefore, here we focused on the thinner endplate connections, and compared the performance of connection with various thicknesses of stiffeners. Thickness of the stiffeners were varied from 6 mm to 12 mm, and to better compare the connection performance, the ring-plate welded connection was added into the comparison. The results indicated that for thinner endplate conditions, even with thick stiffeners (like t_s=12 mm), the connection still have pinched hysteretic loops (Fig. 15). The thicker stiffeners presented slight increasing effect on the moment bearing ability and energy dissipation ability of the connection. But this elevation effect is limited. The reasons may mainly be attributed to the local bending deformation and warping failure at endplate for the thinner endplate connections. Increasing the thickness of the stiffener could slightly alleviate the warping deformation, but could not change this failure mode. However, when the endplate thickness was increased to 14mm, changing the stiffener dimension did not present much difference on the moment-rotation relations. Moreover, compared to the external ring-plate welded connection, the stiffened endplate connections with both 12 mm and 14 mm endplates all had pinching hysteretic loops, where failure modes were still attributed to the local wraping at the endplate. But for blind-bolt endplate connections with 14 mm endplate, the local bending deformation may be limited to certain extent

3.2.4 Effect of stiffener thickness for thick end plate blind-bolt connections

Fig. 16 gives the connection performance of thick

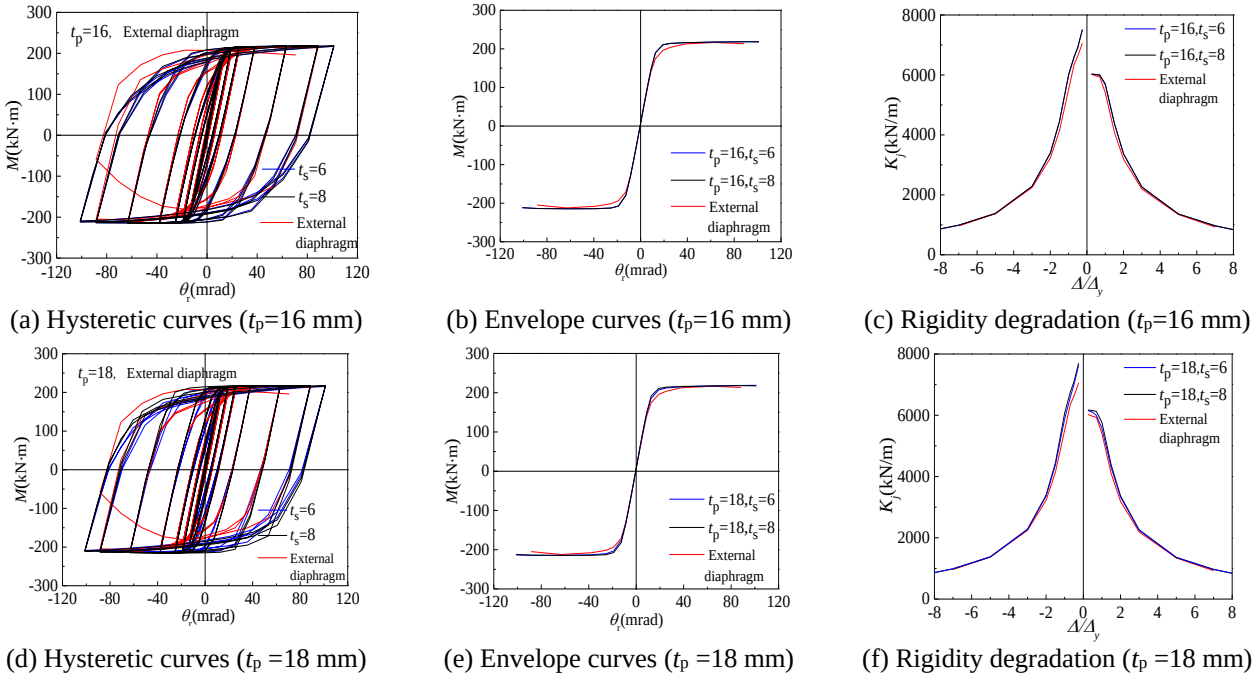

(a) Hysteretic curves (t_p=16 mm) (b) Envelope curves (t_p=16 mm) (c) Rigidity degradation (t_p=16 mm)

(d) Hysteretic curves (t_p =18 mm) (e) Envelope curves (t_p =18 mm) (f) Rigidity degradation (t_p =18 mm)

Fig. 16 The influence of stiffener thickness for thick end plate

Table 4 Beam-column joints classification method of EC3

Connection class	Type of frames	Boundaries of initial stiffness	Boundaries of moment capacities
Pinned	—	$K_e \le 0.5EI_b/L_b$	$M_u \le 0.25M_{bp}$
Semi-rigid	Sway frames (SF)	$0.5EI_b/L_b < K_e < 25EI_b/L_b$	—
	Non-sway frames (NSF)	$0.5EI_b/L_b < K_e < 8EI_b/L_b$	—
Rigid	Sway frames (SF)	$K_e \ge 25EI_b/L_b$	—
	Non-sway frames (NSF)	$K_e \ge 8EI_b/L_b$	—
Partial strength	—	—	$0.25M_{bp} < K_e < M_{bp}$
Full strength	—	—	$M_u \ge M_{bp}$

Note: EI_b and L_b are the flexural rigidity and the length of the steel beam respectively, M_u and M_{bp} are the ultimate moment capacity and design plastic moment resistance of the steel beam respectively

endplate (t_p=16 mm and 18 mm) blind-bolt connections with various thickness stiffeners. These connections all displayed pump hysteretic loops and the moment bearing strength development and energy dissipation ability were all close to the ring-plate welded connection. Results indicated that the thick plate blind-bolt connection strengthened with appropriate stiffeners can provide similar moment strength and seismic performance as that of external diaphragm connection. For the thick endplate blind-bolt connection, the stiffener thickness only had slight influence on the initial period of reloading stages.

3.3 Further evaluation of connection classification

At present, particular specifications for the endplate blind-bolted connections were limited, and no further guidance can be found for the stiffened endplate blind-bolted connections. Then based on the classification method provided by the Eurocode3 (1998, 2003), as summarized in Table 4; the connection rigidity and strength conditions for this kind of connections were asserted, with the results given in Fig. 17. It can be seen that: (1) According to the rigidity classification, the stiffened and unstiffened blind-bolt connections were sorted to semi-rigid connections; (2) Based on the strength classification, only the model DES1 belonged to the partial strength connections, and the other connections were all full-strength connections. It is also found that the rotation capacity of all specimens all satisfied the ductility requirement of no less than 30 mrad for earthquake resistance, which was suggested by FEMA-350 (2000). EC3 gave a broad range for semi-rigid connections, even with strong stiffeners, the blind-bolted connections still belonged to semi-rigid connections and can be only applied in low-rise and mid-rise buildings. Here a more detailed rigidity classification is proposed. The external diaphragm connections were generally regarded as rigid

Table 5 Further classification method of blind bolted endplate connections

Classification	Ratio of initial stiffness (K) and moment capacity (M)	Ratio of energy dissipation (E)	Mode of connection
Semi-rigid	K<0.75 or M<0.75	E<0.40	Unstiffened or thin end plate
Quasi-rigid	0.75<K<0.95 and 0.75<M<0.95	0.40<E<0.55	Thick unstiffened end plate or thin stiffened end plate
Rigid(1)	K >0.95 and M >0.95	0.60<E<0.90	Thick stiffened end plate
Rigid(2)	K >0.95 and M >0.95	0.80<E<0.90	Thicker stiffened end plate

Note: The value of the initial stiffness, moment capacity and energy dissipation are shown in Tables 6 and 7

Table 6 The ultimate moment and the initial rotational stiffness of various models

Model number	Loading direction	t_p	t_s	M_{max} (kN·m)	Percentage[a]	K_e (kN·m /mrad)	Percentage[a]	Classification of connection
DES15	-	—	—	-216.7	100%	17.6	100%	Rigid
	+			212.2	100%	13.7	100%	
DES1	-	12	0	-138.6	64%	13.4	76%	Semi-rigid
	+			135.1	64%	10.8	78%	
DES2	-	18	0	-213.3	98%	16.7	94%	Quasi-rigid
	+			203.6	96%	13.6	99%	
DES3	-	12	8	-204.3	94%	17.1	97%	Quasi-rigid
	+			199.9	94%	12.7	92%	
DES4	-	12	10	-209.7	97%	17.3	95%	Quasi-rigid
	+			205.7	97%	12.9	94%	
DES5	-	12	12	-212.3	98%	17.4	99%	Quasi-rigid
	+			208.0	98%	12.9	94%	
DES6	-	14	0	-187.8	87%	15.2	86%	Semi-rigid
	+			183.9	87%	11.7	85%	
DES7	-	14	6	-218.3	101%	17.6	100%	Rigid
	+			213.3	100%	13.5	98%	
DES8	-	14	8	-218.3	101%	17.6	100%	Rigid
	+			213.4	101%	13.5	98%	
DES9	-	14	10	-219.1	101%	17.7	100%	Rigid
	+			214.3	101%	13.6	99%	
DES10	-	16	0	-196.4	91%	16.4	93%	Semi-rigid
	+			193.9	91%	12.6	92%	
DES11	-	16	6	-218.6	101%	18.6	105%	Rigid
	+			214.5	101%	14.2	104%	
DES12	-	16	8	-218.4	101%	18.5	105%	Rigid
	+			214.5	101%	14.2	104%	
DES13	-	18	6	-218.8	101%	18.9	107%	Rigid
	+			214.5	101%	14.4	105%	
DES14	-	18	8	-218.3	101%	19.0	108%	Rigid
	+			214.6	101%	14.6	106%	

Note: [a] The percentage was calculated by comparing DES1~14 models to DES15 model.

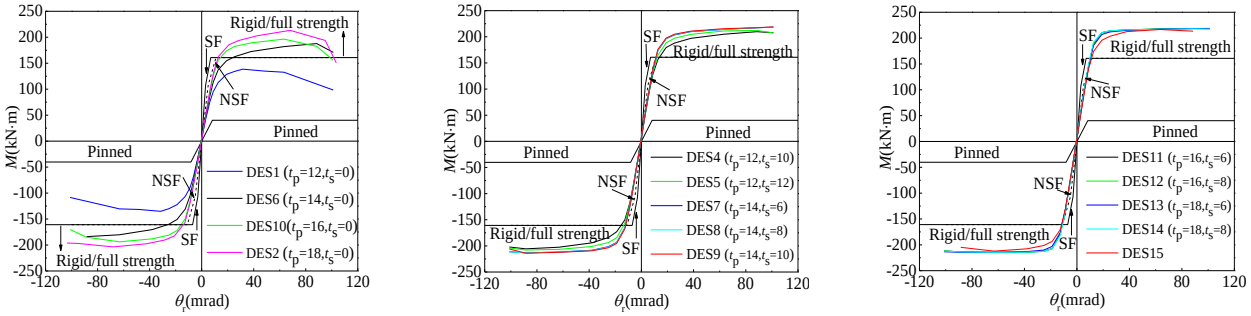

(a) Envelope curves (b) Envelope curves (c) Envelope curves

Fig. 17 Classification of all simulated connections

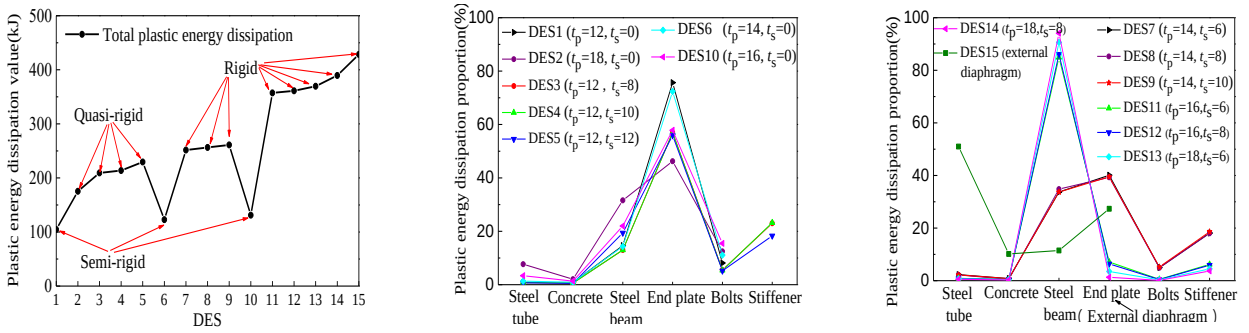

(a) The total plastic energy dissipation

(b) Proportion of plastic energy dissipation of semi-rigid and quasi-rigid joints

(c) Proportion of plastic energy dissipation of various components of rigid joints

Fig. 18 Comparison with plastic energy dissipation of several joints

connections, which was then taken as the benchmark for the rigid connections. Then based on the rigidity, strength and energy dissipation comparisons, a further classification method of blind bolted endplate connections is given in Table 5.

Table 6 gives the moment strength and initial stiffness of all the simulated models, and the classification of different connections under the proposed classification method, the thick stiffened endplate blind-bolt connections with thick stiffeners can be regarded as rigid connections, and part of stiffened blind-bolted connection can be sorted as quasi-rigid connections

3.4 Energy dissipation analysis

The energy dissipation of analyzed connections and the energy dissipation share at different components were obtained from the numerical models, as given in Table 7 and Fig. 18. The external diaphragm connection had the maximum energy dissipation ability. Due to the assembled construction, energy dissipation ability of the stiffened and unstiffened blind-bolt connections was all lower than that of the external diaphragm connection. But for the connections with thick endplate and thick stiffeners, like DES14, the energy dissipation ability could reach about 91% of that in external diaphragm connection. For the semi-rigid and quasi-rigid blind-bolt connection, the end plate was the main energy dissipation source, as shown in Fig. 18(b).

While for connections DMS7~9, the thin endplate construction leaded to the relative low energy dissipation ability, only accounting for about 60% of that in external diaphragm connection. In this condition, the steel beam was not the only energy dissipation source, but also the endplate. For thick endplate connections like DMS11~14, the local bending extent at endplate was small and the plasticity mainly came from the steel beam. Then the energy dissipation ability was high, which accounted for more than 80% of that in external diaphragm connections. Therefore, the rigid connections have the energy dissipation mainly from the steel beam. For the semi-rigid and quasi-rigid connections, the steel beam, the endplate and stiffeners could all participate in the energy dissipation.

4. Conclusions

In this paper, the performance of stiffened endplate blind-bolt connections was studied through 3D finite element simulations. Influence of stiffeners and the combined effect with endplate were discussed through parametric analyses. The following conclusions could be drawn on this research work:

(1) The finite element can well predict the moment-rotation relations (both monotonic loading and cyclic loading), skeleton curves, failure modes, and strain development at different connection components.

Table 7 Total plastic energy dissipation and the share at different components

Model No	t_p	t_s	Energy dissipation (E) and proportion (kJ)	Steel tube	Concrete	Bolts	Steel beam	End plate	Stiffener or external diaphragm	Classification of connection
DES1	12	0	104.6(24%)	0.7%	0.8%	8.1%	14.6%	75.7%	/	Semi-rigid
DES2	18	0	175.3(41%)	7.7%	2.0%	12.5%	31.6%	46.2%	/	Quasi-rigid
DES3	12	8	209.3(49%)	0.9%	0.6%	5.5%	13.0%	57.0%	23.0%	Quasi-rigid
DES4	12	10	213.7(50%)	0.9%	0.6%	5.4%	13.0%	56.9%	23.2%	Quasi-rigid
DES5	12	12	229.5(54%)	0.7%	0.5%	5.2%	19.4%	55.9%	18.3%	Quasi-rigid
DES6	14	0	122.8(29%)	1.3%	0.9%	11.1%	14.3%	72.4%	/	Semi-rigid
DES7	14	6	251.5(59%)	2.3%	0.8%	5.0%	33.7%	40.1%	18.1%	Rigid
DES8	14	8	256.4(60%)	2.2%	0.8%	4.9%	34.8%	39.3%	18.0%	Rigid
DES9	14	10	261.0(61%)	2.2%	0.8%	5.2%	33.7%	39.5%	18.6%	Rigid
DES10	16	0	131.1(31%)	3.4%	1.3%	15.5%	22.0%	57.8%	/	Semi-rigid
DES11	16	6	357.2(83%)	0.9%	0.4%	0.5%	84.9%	7.1%	6.2%	Rigid
DES12	16	8	361.1(84%)	0.8%	0.4%	0.4%	86.1%	6.4%	5.9%	Rigid
DES13	18	6	369.6(86%)	0.7%	0.4%	0.3%	90.6%	3.5%	4.5%	Rigid
DES14	18	8	389.5(91%)	0.5%	0.3%	0.1%	94.1%	1.3%	3.7%	Rigid
DES15	/	/	428.4(100%)	51%	10.2%	/	11.5%	/	27.4%	Rigid

It is shown that the FEA models could be used to predict the performance of blind bolted moment connections with a proper precision.

(2) The vertical stiffeners can effectively alleviate the local bending deformation at endplate. The moment bearing and seismic performance of the blind-bolt connections were closely related to the endplate and stiffeners. In thin endplate cases, the connection mainly displayed pinching behaviors with obvious local bending happened at the endplate. Increasing the stiffeners can slightly improve the mechanical behaviors of the connections. In thick endplate cases, the presence of stiffeners can ensure the plasticity mainly to happen in steel beams, leading to full hysteretic loops.

(3) Along with joint connection classification in EC3, a more detailed rigidity classification method was proposed. In the proposed method, the ring-plate welded connection was taken as the benchmark of rigid connections. Then semi-rigid, quasi-rigid and rigid connections were put forwarded. According to the new classification, the thick endplate blind-bolt connections strengthened with thick stiffeners can almost achieve the same stiffness and moment bearing ability of ring-plate welded connections, thus can be regarded as rigid connection.

(4) For the rigid connections within the proposed joint classification, the energy dissipation mainly happened at steel beams. For the semi-rigid and quasi-rigid connections, the extended endplate, stiffeners and steel beam would all participate in the energy dissipation.

Acknowledgments

This research is supported by the National Key Research Program of China, Grant No. 2017YFC0703404, and the National Natural Science Foundation of China, Grant No.51578548. Science Fund for Distinguished Young Scholars of Hunan, Grant No. 2019JJ20029.

References

A. AISC. (2010), "Prequalified connections for special and intermediate steel moment frames for seismic applications", American Institute of Steel Construction, Chicago, IL.

Beena, K., Naveen, K. and Shruti, S. (2017), "Behaviour of bolted connections in concrete-filled steel tubular beam-column joints", *Steel Compos. Struct.*, **25**(4), 443-456. https://doi.org/10.12989/scs.2017.25.4.443.

D'Aniello, M., Tartaglia, R. Costanzo, S. and Landolfo, R. (2017), "Seismic design of extended stiffened end-plate joints in the framework of Eurocodes", *J. Constr Steel Res.*, **128**, 512-527. https://doi.org/10.1016/j.jcsr.2016.09.017.

Da Silva, L.S., de Lima, L.R., da SVellasco, P.C.G. and de Andrade, S.A. (2004). "Behaviour of flush end-plate beam-to-column joints under bending and axial force", *Steel Compos. Struct.*, **4**(2), 77-94. https://doi.org/10.12989/scs.2004.4.2.077.

Dessouki, A.K., Youssef, A.H. and Ibrahim, M.M. (2013), "Behavior of I-beam bolted extended end-plate moment connections", *Ain. Shams. Eng. Jour.*, **4**(4), 685-699. https://doi.org/10.1016/j.asej.2013.03.004.

Ding, F.X., Yin, G.A., Jiang, L.Z. and Bai, Y. (2018), "Composite frame of circular CFST column to steel-concrete composite beam under lateral cyclic loading", *Thin-Wall. Struct.*, **122** (1), 137-146. https://doi.org/10.1016/j.tws.2017.10.022.

Ding, F.X., Yin, G.A., Wang, L.P., Hu, D. and Chen, G.Q. (2017), "Seismic performance of a non-through-core concrete between concrete-filled steel tubular columns and reinforced concrete beams", *Thin-Wall. Struct.*, **110**(1), 14-26. https://doi.org/10.1016/j.tws.2016.10.014.

Ding, F.X., Yin, G.A., Wang, H. B., Wang, L. and Guo, Q. (2017), "Behavior of headed shear stud connectors subjected to cyclic loading", *Steel Compos. Struct.*, **25**(6), 705-716.

https://doi.org/10.12989/scs.2017.25.6.705.

Ding, F.X., Luo, L. Zhu, J. Wang, L. and Yu, Z.W. (2018), "Mechanical behavior of stirrup-confined rectangular CFT stub columns under axial compression", *Thin-Wall. Struct.*, **124,** 136-150. https://doi.org/10.1016/j.tws.2017.12.007.

Ding, F.X., Ying, X.Y. Zhou, L.C. and Yu, Z.W. (2011a), "Unified calculation method and its application in determining the uniaxial mechanical properties of concrete", *Front. Archit. Civ Eng. China*., **5**(3), 381-393. https://doi.org/10.1007/s11709-011-0118-6.

Eurocode 3 (1998), ENV - 1993-1-1:1992/A2, Annex J, Design of Steel Structures - Joints in Building Frames.CEN, European Committee for Standardisation, Document CEN/TC 250/SC 3, Brussels.

Eurocode 3 (2003), prEN 1993-1-8: 2003, Part 1.8: Design of Joints, Eurocode 3: Design of Steel Structures,

Stage 49 draft., 5 May 2003. CEN, European Committee for Standardisation, Brussels.

FEMA-350. (2000), "Recommended Seismic Design Criteria for New Steel Moment-frame Buildings, SAC Joint Venture, Federal Emergency Management Agency, Washington D.C.

Guo, B., Gu, Q. and Liu, F. (2006), "Experimental behavior of stiffened and unstiffened end-plate connections under cyclic loading", *J. Struct. Eng*., **132**(9), 1352-1357.

Korol, R.M., Ghobarah, A. and Mourad, S. (1993), "Blind Bolting W-Shape Beams to HSS Columns", *J. Struct. Eng*., **119**(12)**,** 3463-3481. https://doi.org/10.1061/(ASCE)0733-9445(1993)119:12(3463).

Ma, H.W., Jiang, WS. and Cho, CD. (2011), "Experimental study on two types of new beam-to-column connections", *Steel Compos. Struct*., **11**(4), 291-305.

Morrison, M., Quayyum, S. and Hassan, T. (2017), "Performance enhancement of eight bolt extended end-plate moment connections under simulated seismic loading", *Eng. Struct.*, **151,** 444-458. https://doi.org/10.1016/j.engstruct.2017.08.040.

Mourad, S., Ghobarah, A. and Korol, R.M. (1995), "Dynamic response of hollow section frames with bolted moment connections", *Eng. Struct.*, **17**(10), 737-748. https://doi.org/10.1016/0141-0296(95)00002-O.

Murray, T.M. Sumner, E.A. AISC design guide series 4. (2003), "Extended end-plate moment connections", in: A.I.o.S. Construction (Ed.), Chicago.

Tao, Z., Li, W. Shi, B.L. and Han, L.H. (2017), "Behaviour of bolted end-plate connections to concrete-filled steel columns", *J. Constr Steel Res.*, **134,** 194-208. https://doi.org/10.1016/j.jcsr.2017.04.002.

Tartaglia, R., D'Aniello, M. Rassati, G.A. Swanson, J.A. and Landolfo, R. (2018), "Full strength extended stiffened end-plate joints: AISC vs recent European design criteria", *Eng. Struct.*, **159**, 155-171. https://doi.org/10.1016/j.engstruct.2017.12.053.

Tartaglia, R., D'Aniello, M. Zimbru, M. and Landolfo, R. (2018), "Finite element simulations on the ultimate response of extended stiffened end-plate joints", *Steel Compos. Struct*., **27**(6), 727-745. https://doi.org/10.12989/scs.2018.27.6.727.

Thai, H.T., Uy, B. and Aslani, F. (2017), "Behaviour of bolted endplate composite joints to square and circular CFST columns", *J. Constr. Steel Res.*, **131**, 68-82. https://doi.org/10.1016/j.jcsr.2016.12.022.

Tsai, K.C. and Popov, E.P. (1990), "Cyclic behavior of end-plate moment connections", *J. Struct. Eng*., **116**(11), 2917-2930. https://doi.org/10.1061/(ASCE)0733-9445(1990)116:11(2917).

Wang, J.F. and Spencer Jr., B.F. (2013), "Experimental and analytical behavior of blind bolted moment connections", *J. Constr. Steel Res.*, **82,** 33-47. https://doi.org/10.1016/j.jcsr.2012.12.002.

Wang, J.F. and Chen, L.P. (2012), "Experimental investigation of extended end plate joints to concrete-filled steel tubular columns", *J. Constr. Steel Res.*, **79**, 56-70. https://doi.org/10.1016/j.jcsr.2012.07.016.

Wang, J.F, Zhang, L. and Spencer Jr., B.F. (2013), "Seismic response of extended end plate joints to concrete-filled steel tubular columns", *Eng. Struct.*, **49,** 876-892. https://doi.org/10.1016/j.engstruct.2013.01.001.

Wang, J., Uy, B. and Li, D.X. (2018), "Analysis of demountable steel and composite frames with semi-rigid bolted joints", *Steel Compos. Struct*., **28**(3)**,** 363-380. https://doi.org/10.12989/scs.2018.28.3.363.

Wang, P., Pan, J.R., Wang, Z. and Chen, S.Z. (2018). "Experimental and analytical behavior of stiffened angle joints", *Steel Compos. Struct*., **26**(1), 67-78. https://doi.org/10.12989/scs.2018.26.1.067.

Wang, W., Li, L. Chen, D.B. and Xu, T. (2018), "Progressive collapse behaviour of extended endplate connection to square hollow column via blind Hollo-Bolts", *Thin-Wall. Struct*., **131,** 681-694. https://doi.org/10.1016/j.tws.2018.07.043.

Wang, W., Li, M.X., Chen, Y.Y. and Jian, X.G. (2017), "Cyclic behavior of endplate connections to tubular columns with novel slip-critical blind bolts", *Eng. Struct.*, **148,** 949-962. https://doi.org/10.1016/j.engstruct.2017.07.015.

Wang, J., Zhu, H.M., Uy, B., Patel, V., Aslani, F. and Li, D.X. (2018), "Moment-rotation relationship of hollow-section beam-to-column steel joints with extended end-plates", *Steel Compos. Struct*., **29**(6)**,** 717-734. https://doi.org/10.12989/scs.2018.29.6.717.

Wang, Z.Y. and Wang, Q.Y. (2016), "Yield and ultimate strengths determination of a blind bolted endplate connection to square hollow section column", *Eng. Struct.*, **111,** 345-369. https://doi.org/10.1016/j.engstruct.2015.11.058.

Waqas, R., Uy, B. and Thai, H.T. (2019), "Experimental and numerical behaviour of blind bolted flush endplate composite connections", *J. Constr. Steel Res.*, **153,** 179-195. https://doi.org/10.1016/j.jcsr.2018.10.012.

Yao, H., Goldsworthy, H. and Gad, E. (2008). "Experimental and numerical investigation of the tensile behavior of blind-bolted T-stub connections to concrete-filled circular columns", *J. Struct Eng*., **134**(2), 198-208. https://doi.org/10.1061/(ASCE)0733-9445(2008)134:2(198).

Suita, K. and Tanaka, T. (2000). "Flexural strength of beam web to square tube column joints", *Kou kouzou rombunshuu*, **7**(26), 51-58.

Yu, Y.J, Chen, Z.H. and Wang, X.D. (2015), "Effect of column flange flexibility on WF-beam to rectangular CFT column connections", *J. Constr. Steel Res*., **106**, 184-197. https://doi.org/10.1016/j.jcsr.2014.12.008.

Yu, Y.J., Wang, X.D. and Chen, Z.H. (2017), "Evaluation on steel cyclic response to strength reducing heat treatment for seismic design application", *Constr. Build. Mater*., **140**, 468-484. https://doi.org/10.1016/j.conbuildmat.2017.02.088.

Zhang, Z., Wang, J., Li, B. and Zhao, C. (2019), "Seismic tests and numerical investigation of blind-bolted moment CFST frames in-filled with thin-walled SPSWs", *Thin-Wall. Struct*., **134,** 347-362. https://doi.org/10.1016/j.tws.2018.10.009.

BU